Hindawi
Journal of Sensors
Volume 2024, Article ID 9819425, 1 page
https://doi.org/10.1155/2024/9819425

Retraction

Retracted: Sensor-Based Exercise Rehabilitation Robot Training Method

Journal of Sensors

Received 23 January 2024; Accepted 23 January 2024; Published 24 January 2024

This article has been retracted by Hindawi following an investigation undertaken by the publisher [1]. This investigation has uncovered evidence of one or more of the following indicators of systematic manipulation of the publication process:

(1) Discrepancies in scope
(2) Discrepancies in the description of the research reported
(3) Discrepancies between the availability of data and the research described
(4) Inappropriate citations
(5) Incoherent, meaningless and/or irrelevant content included in the article
(6) Manipulated or compromised peer review

The presence of these indicators undermines our confidence in the integrity of the article's content and we cannot, therefore, vouch for its reliability. Please note that this notice is intended solely to alert readers that the content of this article is unreliable. We have not investigated whether authors were aware of or involved in the systematic manipulation of the publication process.

Wiley and Hindawi regrets that the usual quality checks did not identify these issues before publication and have since put additional measures in place to safeguard research integrity.

We wish to credit our own Research Integrity and Research Publishing teams and anonymous and named external researchers and research integrity experts for contributing to this investigation.

The corresponding author, as the representative of all authors, has been given the opportunity to register their agreement or disagreement to this retraction. We have kept a record of any response received.

References

[1] S. Xie and J. Zhang, "Sensor-Based Exercise Rehabilitation Robot Training Method," *Journal of Sensors*, vol. 2023, Article ID 7881084, 9 pages, 2023.

Hindawi
Journal of Sensors
Volume 2023, Article ID 7881084, 9 pages
https://doi.org/10.1155/2023/7881084

Research Article

Sensor-Based Exercise Rehabilitation Robot Training Method

Shangsen Xie[1] **and Jingru Zhang**[2]

[1]*School of Physical Education, Fuyang Normal University, Fuyang, Anhui 236037, China*
[2]*School of Information Engineering, Fuyang Normal University, Fuyang, Anhui 236037, China*

Correspondence should be addressed to Jingru Zhang; 11231518@stu.wxic.edu.cn

Received 10 July 2022; Revised 6 August 2022; Accepted 22 August 2022; Published 24 March 2023

Academic Editor: Haibin Lv

In order to provide convenience for rehabilitation doctors to formulate rehabilitation plans for patients, this paper proposes a training method for exercise rehabilitation robots based on sensors. In this research, the customized wearable sensor and universal mobile terminal are used as the hardware. Based on the sensor, the motion capture algorithm and motion reconstruction algorithm are developed. The table of experimental results shows that the cost can be saved by using the sensor, and the data can be captured accurately, which can meet the needs of rehabilitation medicine for motor function evaluation and training guidance. The range of motion of the joint and the manual measurement value are within 5°, which can meet the needs of rehabilitation medicine for motor function evaluation and training guidance. The system delay is less than 0.5 s, which has good real-time performance and can respond quickly to emergencies, ensuring the safety of patients' out-of-hospital rehabilitation. The training method of motion rehabilitation robot based on sensor is helpful for rehabilitation doctors to carry out statistical data of functional evaluation and is of great significance for rehabilitation doctors to make training plans for patients and carry out rehabilitation training.

1. Introduction

With the rapid development of information technology, traditional medical equipment is constantly developing in the direction of intelligence, while rehabilitation robots are combined with the development results of multiple disciplines and are widely used in medical diagnosis and treatment, clinical surgery, rehabilitation medicine, and other related medical fields [1].

Sensor technology is one of the important basic technologies of modern information technology. With the development of modern detection, control, and automation technology, sensor technology is becoming more and more mature. People pay more and more attention to it, and it is widely used in various fields [2]. The application of sensor technology in the field of rehabilitation medicine provides a new impetus for the development of rehabilitation evaluation and treatment technology [3].

As a medical robot used in the field of rehabilitation medicine, rehabilitation robot can help patients with exercise or cognitive function training and to some extent solve the problems of fatigue and differences in multiple training in artificial rehabilitation training [4]. According to their different functional training, rehabilitation robots can be divided into motion disability rehabilitation robots and cognitive disability rehabilitation robots. According to the difference of the trained limbs, the rehabilitation robot for movement disorders can be divided into upper limb rehabilitation robot and lower limb rehabilitation robot. The upper limb rehabilitation robot mainly assists the exercise training of the patient's shoulder, elbow, hand, and other upper limb joints. Through the active and passive rehabilitation training, the strength of the patient's muscle tissue and the flexibility of the hand to do fine movements are strengthened, and the force, torque, and other sensors are installed to evaluate the process and results of the rehabilitation training. The lower limb rehabilitation robot is mainly the lower limb exoskeleton robot, which focuses on the rehabilitation training of patients such as auxiliary standing, balance and walking. If the patient's rehabilitation training can be captured by

the sensor for a long time to form statistical data and then evaluated by the rehabilitation doctor according to the statistical value, the results are of great significance for the development of rehabilitation medicine and the evaluation of interventional treatment effect. Therefore, the rehabilitation training robot has become one of the research hotspots in medical robots in recent years. Figure 1 shows the interaction method in the rehabilitation training robot.

2. Literature Review

With the development of science and technology, sports rehabilitation robot has achieved unprecedented development in recent years. By making use of the characteristics of robots such as high precision, high repeatability, and customization and combining with the basic idea of sports rehabilitation therapy, robots are applied to sports rehabilitation, resulting in a large number of sports rehabilitation robots, including robots for rehabilitation training of upper limbs, lower limbs, ankles, and feet. Among them, sports rehabilitation robots based on wearable exoskeletons have been widely studied and applied in recent years, as shown in Table 1.

Dionisio and others analyzed and compared the monitoring data of 10 parts of the manikin measured by Kinect sensor and the most advanced markable 3D camera (MBC) by using the principal component analysis method and found that Kinect sensor has high accuracy in identifying the whole body movement mode, and the price is low, which is more suitable for promotion and application in clinical rehabilitation training [5]. Chen and others designed a knee flexion angle measurement system based on resistance sensor. The system records the resistance changes during movement through the resistance sensor installed in the wearable knee pad and then calculates the knee flexion angle. It can be used by rehabilitation professionals and patients with knee dysfunction to monitor the knee flexion angle in real time during training, so as to improve the process of rehabilitation evaluation and rehabilitation training [6]. Jang and others developed an integrated sensor shoe composed of pressure and bending sensors. This shoe can send the gait information collected during walking to the server so that doctors can visually observe the changes of foot weight and ankle angle when patients walk [7]. Duan and others monitored the daily energy consumption of hemiplegic patients by placing a swp2a system composed of 2 accelerometers, 1 skin electric response sensor, heat sensor, skin temperature sensor, and 1 ambient temperature sensor at the midpoint of the healthy triceps brachii. Combined with the individual conditions of the patients, such as height, body mass, and other information, the intensity of each exercise of the subjects is calculated through a unique formula, so as to achieve the purpose of monitoring the energy consumption of hemiplegic patients [8]. Yu and others used inertia and air pressure sensors to make a device similar to a wrist watch. After the patient wears this device on the wrist, the metabolic equivalent of the patient's activities of daily living can be monitored in real time according to the information received by the sensor. Compared with the previous equipment for monitoring the amount of metabolism, it is simpler and will not affect the patient's activities [9].

In view of the above problems, considering that the optical tracking equipment is difficult to play a role in various complex environmental conditions, in this paper, we developed a MEMS device and motion capture algorithm based on Magnetometer and inertial sensor to realize the research on the training method of motion rehabilitation robot.

3. Method

3.1. Research Scheme

3.1.1. Equipment Composition. The core component of the wearable sensor device described in this paper is the yd122 sensor, which is a MEMS sensor [10]. Each sensor is integrated with a 9-axis mpu9250 chip, which can measure the acceleration, angular velocity, and magnetic field strength of three axes [11]. The STM32 microprocessor inside the sensor filters the measured acceleration, angular velocity, and magnetic force values into four elements or Euler angles representing the current attitude. In addition, the yd122 master sensor has its own battery and Bluetooth module, which can be used alone or in cascade with a yd122 slave sensor. When in use, a single master sensor is fixed to the chest of the subject through a strap, and 4 sets of master + Slave sensors are, respectively, bound to the outside of the left and right thighs, the outside of the left and right lower legs, the outside of the left and right upper arms, and the outside of the left and right forearms, a total of 9. In addition to the sensors, the device also includes a general-purpose mobile terminal, which is used to obtain the data of 9 sensors and reconstruct the motion state.

In order to minimize the quality of the exoskeleton and improve the response speed of start and stop, 6061 aluminum alloy is selected as the part material of the exoskeleton manipulator [12]. At the same time, in order to improve the wearing comfort, the shoulder structure is installed on the rack, and the patient does not have to bear the quality of any part after wearing. According to the weight of exoskeleton, combined with adult weight statistics and clinical rehabilitation training experience, the dynamic parameters required for each degree of freedom are selected, as shown in Table 2.

3.1.2. Motion Capture Algorithm. The posture change of human body can be decomposed into the roll angle, heading angle, and pitch angle of trunk, head, and limbs. After wearing the sensor device, the sensor is synchronized with human motion, and the measured changes of magnetic field, acceleration, and angular velocity can be used to reconstruct the motion state. In this experiment, the movements of both sides of the trunk and limb joints of the subjects were mainly tracked (usually the limbs on both sides of the joints have obvious movement pattern differences), while the movements of the head and the ends of the limbs were ignored. In addition, the trunk is also assumed as a whole, regardless of the flexion and extension of the spine.

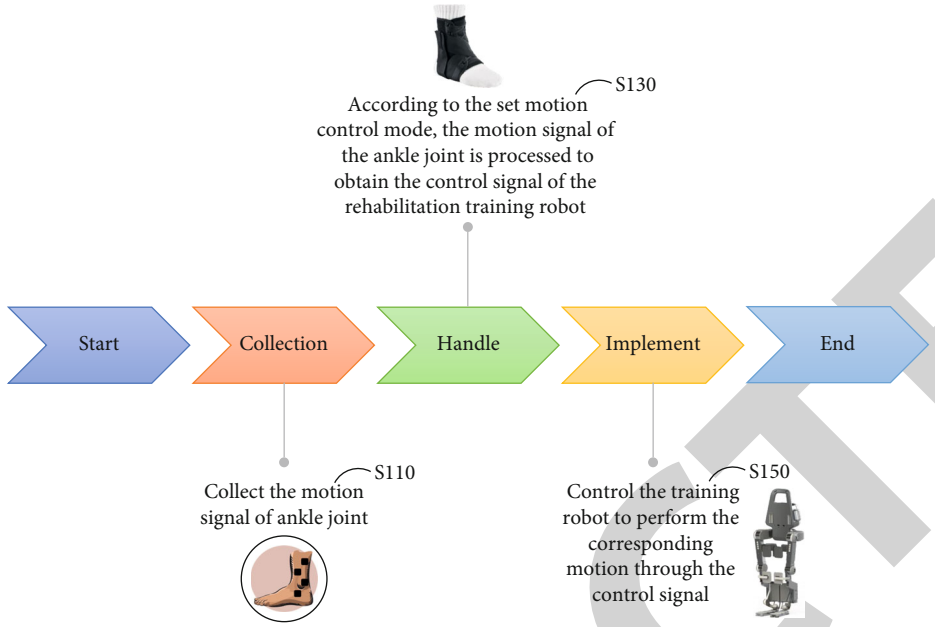

Figure 1: Interaction method in rehabilitation training robot.

Table 1: Some common exercise rehabilitation training robots and their functions.

Robot name	Configuration type	Applicable parts	Freedom	Active training	Passive training	Impedance training	Seme	Game interaction
MT-MANUS	End pull type	Shoulder, elbow	3	√	√			√
ARMin	Exoskeleton type	Shoulder, elbow, wrist	6		√	√		√
Harmon	Exoskeleton type	Simultaneous training of both upper limbs	12	√	√			
Co-Exos	Exoskeleton type	Upper limb	6	√	√		√	
Lokomat	Exoskeleton type	The legs	4	√	√	√		√
Ekso	Exoskeleton type	The legs	4		√			
Indego	Exoskeleton type	The legs	4		√			
HAL	Exoskeleton type	The legs	6	√	√		√	
AIDER	Exoskeleton type	The legs	6	√	√		√	
HemiGo	Exoskeleton type	The legs	6	√	√	√		√
GEMS-HI	Exoskeleton type	Hip joint	1	√				
GEMS-K1	Exoskeleton type	Knee joint	1	√				
GEMS-A1	Exoskeleton type	Ankle joint	1	√				
RutgersAnkle	End pull type	Ankle joint	1	√	√			√
PAFO	Exoskeleton type	Ankle joint	1		√			
ReStore	Exoskeleton type	Ankle joint	1	√	√	√		

Table 2: Dynamic parameters of two degrees of freedom.

Freedom	Torque (N.m)	Maximum speed (r/min)	Motor power (W)
Elbow flexion/extension	23	30	100
Shoulder flexion/extension	35	30	200
Shoulder abduction/adduction	41	30	200

In the motion capture algorithm of multisensor data fusion, the wearing position of the sensor has a great impact on the algorithm design. The forearm and upper arm can change freely in three degrees of freedom, and the speed is fast, and the direction cannot be predicted. The movement of thigh and calf is mainly the change of flexion and extension direction and orientation, and the deflection (roll) to both sides is less, and the range is small. The trunk part is mainly translational, with less large forward tilt, backward tilt, and lateral bending, and the movement is slow. Here, taking the sensor placed on the thigh as an example, the motion capture algorithm implemented in this device is introduced.

The thigh flexion and extension angle θ is defined as the angle between the y-axis and the opposite direction of gravity, and the thigh swing velocity (angular velocity) is $v = d\theta/dt$ [13, 14]. Considering that the swinging speed of the thigh is slow, the sampling rate of the sensor is 25 Hz, the angular velocity changes very little within the sampling interval (the change value can be simulated by the system noise), and the filter uses the constant angular velocity model to deduce. The state update equation is

$$\begin{bmatrix} \theta_k \\ v_k \\ a_k \\ c_k \end{bmatrix} = \begin{bmatrix} 1 & t_s & 0 & 0 \\ 0 & 1 & 0 & 0 \\ 0 & 0 & 1 & 0 \\ 0 & 0 & 0 & 1 \end{bmatrix} \cdot \begin{bmatrix} \theta_{k-1} \\ v_{k-1} \\ a_{k-1} \\ c_{k-1} \end{bmatrix} + \begin{bmatrix} w_\theta \\ w_v \\ w_a \\ w_c \end{bmatrix}, \tag{1}$$

where the subscript represents time k and time $k-1$, TS is the sampling interval, andw_θ, w_v, w_a and w_c are the system noise of each state variable, respectively [15]. It can be assumed that they are independent 0-means Gaussian noise, and their distribution function is

$$P(w_\theta, w_v, w_a, w_c) \sim N(0, Q). \tag{2}$$

The calculation method of Q is

$$Q = \begin{bmatrix} Q_\theta & t_s & 0 & 0 \\ 0 & Q_v & 0 & 0 \\ 0 & 0 & Q_a & 0 \\ 0 & 0 & 0 & Q_c \end{bmatrix}. \tag{3}$$

Q_θ, Q_v, Q_a, and Q_c are the variances of each state variable [16]. The measured value of the sensor is the acceleration D in the x-axis direction and the acceleration B in the y-axis direction. The relationship between the observed value and the state variable (observation equation) is

$$\begin{cases} d_k = -g \sin\theta_k + a_k \sin\theta_k + c_k \cos\theta_k + w_d, \\ b_k = -g \cos\theta_k + a_k \cos\theta_k - c_k \sin\theta_k - r v_k^2 + w_b, \end{cases} \tag{4}$$

where w_d and w_b are the observation noise and R is the distance from the hip joint to the sensor. Similarly, it is assumed that the observation noise is Gaussian noise with independent 0-means [17]:

$$P(w_d, w_b) \sim N(0, R), \tag{5}$$

where $R = \begin{bmatrix} R_d & 0 \\ 0 & R_b \end{bmatrix}$ is the covariance matrix of the observation noise, and R_b and R_d are the variances of the measured values. Equation (4) is written into a matrix format as shown in the following formula [18]:

$$\begin{bmatrix} d_k \\ b_\alpha \end{bmatrix} = h(\theta_k, v_k, a_k, c_k) + \begin{bmatrix} w_d \\ w_b \end{bmatrix}. \tag{6}$$

The observation equation in Equations (4) and (5) is not linear, so the Kalman equation cannot be derived directly. It needs to be locally linearized, and the partial derivative of function h to each state variable is obtained, that is, $H = \alpha h / (\alpha(\theta_k v_\lambda, a_k, c_k))$ obtains the following equation:

$$H = \begin{bmatrix} -g\cos\theta_k + a_k\cos\theta_k - c_k\sin\theta_k & 0 & \sin\theta_k & \cos\theta_k \\ -g\cos\theta_k - a_k\sin\theta_k - c_k\cos\theta_k & -2rv_k & \cos\theta_k & -\sin\theta_k \end{bmatrix}. \tag{7}$$

Local linearization shall be carried out according to the following equation:

$$\begin{bmatrix} d_k \\ b_k \end{bmatrix} = \begin{bmatrix} \tilde{d}_k \\ \tilde{b}_k \end{bmatrix} + H \cdot \begin{bmatrix} \theta_k - \widetilde{\theta}_k \\ v_\alpha - \tilde{v}_k \\ a_k - \tilde{a}_k \\ c_k - \tilde{c}_k \end{bmatrix} \begin{bmatrix} w_d \\ w_k \end{bmatrix}, \tag{8}$$

where $\tilde{d}_k$ and $\widetilde{b}_k$ are the estimated values of d_k and b_k and $\widetilde{\theta}_k$, $\tilde{v}_k$, $\tilde{a}_k$, and $\tilde{c}_k$ are the estimated values of θ_k, v_k, a_k, and c_k, respectively. After obtaining the posterior predicted value of the state variable, update the covariance matrix of the estimated value of the state variable according to the following equation:

$$\begin{aligned} P_k &= \begin{bmatrix} P_\theta & t_s & 0 & 0 \\ 0 & P_v & 0 & 0 \\ 0 & 0 & P_a & 0 \\ 0 & 0 & 0 & P_c \end{bmatrix} \\ &= E\left\{ \begin{bmatrix} \theta_k - \widetilde{\theta}_k \\ v_k - \tilde{v}_k \\ a_k - \tilde{a}_k \\ c_k - \tilde{c}_k \end{bmatrix} \cdot \left[\theta_k - \widetilde{\theta}_k v_k - \tilde{v}_k a_k - \tilde{a}_k c_k - \tilde{c}_k \right] \right\}. \end{aligned} \tag{9}$$

The above steps are recursive derivation of Kalman filter. In actual use, it is necessary to estimate the state variables, system

noise, observation noise, and covariance matrix (see initialization parameter settings and recursive calculation examples). Taking time $k-1$ as an example, the prior prediction of time k according to the state equation is shown in Equation (10), the parameter with wave line on the right side of the equation is the filter estimation value of time $k-1$, and the subscript $(k \mid k-1)$ represents the one-step prediction from time $k-1$ to time K:

$$\begin{bmatrix} \theta_{(k|k-1)} \\ v_{(k|k-1)} \\ a_{(k|k-1)} \\ c_{(k|k-1)} \end{bmatrix} = \begin{bmatrix} 1 & t_s & 0 & 0 \\ 0 & 1 & 0 & 0 \\ 0 & 0 & 1 & 0 \\ 0 & 0 & 0 & 1 \end{bmatrix} \cdot \begin{bmatrix} \widetilde{\theta}_{k-1} \\ \tilde{v}_{k-1} \\ \tilde{a}_{k-1} \\ \tilde{c}_{k-1} \end{bmatrix}. \tag{10}$$

At the same time, the covariance matrix is predicted in one step, as shown in the following equation:

$$P_{(kk-1)} = A\tilde{P}_{k-1}A^T + Q, \tag{11}$$

where $A = \begin{bmatrix} 1 & t_s & 0 & 0 \\ 0 & 1 & 0 & 0 \\ 0 & 0 & 1 & 0 \\ 0 & 0 & 0 & 1 \end{bmatrix}$ is the state transition matrix of Equation (1). Single step prediction of observed values is

$$\begin{cases} d_{(k|k-1)} = -g \sin\theta_{(k|k-1)} + a_{(k|k-1)} \sin\theta_{(k|k-1)} + c_{(k|k-1)} \cos\theta_{(k|k-1)} \\ b_{(k|k-1)} = -g \cos\theta_{(k|k-1)} + a_{(k|k-1)} \cos\theta_{(k|k-1)} - c_{(k|k-1)} \sin\theta_{(k|k-1)} - rv^2_{(k|k-1)} \end{cases}. \tag{12}$$

The Kalman gain is derived from multiple covariance matrices and locally linearized observation functions, as shown in the following equation [19]:

$$K_k = P_{(k|k-1)}H^T\left(HP_{(k|k-1)}H^T + R\right)^{-1}. \tag{13}$$

As shown in Equation (14), the estimated value of the state variable at time k is obtained by weighting the two estimated values by the Kalman gain.

$$\begin{bmatrix} \widetilde{\theta}_k \\ \tilde{v}_k \\ \tilde{a}_k \\ \tilde{c}_k \end{bmatrix} = \begin{bmatrix} \theta_{(k|k-1)} \\ v_{(k|k-1)} \\ a_{(k|k-1)} \\ c_{(k|k-1)} \end{bmatrix} + K_k \begin{bmatrix} d_k - d_{(\wedge|k-1)} \\ b_k - b_{(\wedge|k-1)} \end{bmatrix} \tag{14}$$

Finally, the covariance matrix of the estimated value of the state variable is updated to prepare for filtering at $k+1$, as shown in the following equation:

$$P_k = [1 - K_kH]P_{(k\mu-1)}. \tag{15}$$

The above is the algorithm for tracking the pitch angle of the thigh. This algorithm is also applicable to the legs with similar motion modes. According to the suggestion of the rehabilitation doctor, the pitching and rolling motions of the trunk are small and change slowly. The system obtains them by triangulation according to the components of the gravity component on each axis, and the azimuth of the trunk is also obtained by triangulation of the magnetometer component. The actions of the forearm and upper arm are relatively complex. The Kalman filter similar to the above is used in the equipment for tracking. The principle is the same, but the dimensions of variables and matrices in the state update equation and observation equation are greatly increased. The Kalman filter used in the tracking algorithm is a filtering algorithm without system delay. The filtering value of the current state parameter can be obtained after the new measured value is obtained at time K. For the microprocessor with strong computing power, the data filtering can be completed within a sampling interval.

3.2. Joint Control Experiment. Since the mirror control and synchronous control are only different in motion control mode, and the process of upper limb motion data processing and transformation is basically similar, only the single joint somatosensory mirror control is experimentally analyzed here. The experimenter's right arm (affected limb) wears an exoskeleton mechanical arm, stands at a distance of 2.0~2.5 m from Kinect, and faces Kinect. The left arm (healthy limb) performs slow shoulder abduction, forward flexion, and elbow flexion single joint movements. Kinect collects the joint angle of the left arm, which is converted into control signals through the upper computer processing program, and the somatosensory control exoskeleton mechanical arm drives the right arm to perform mirror motion [20].

In order to further study the "follow-up" performance of each axis in the mirror mode, extract the upper limb motion data and the actual position of the motor within 15 s (the extraction frequency is 30 Hz), and draw the change curve, as shown in Figures 2(a), 2(b), and 2(c). At the beginning of the movement, there is a large error between the joint angle of the control arm and the joint angle of the exoskeleton manipulator. This is because the first group of angles calculated from the somatosensory data obtained by Kinect are

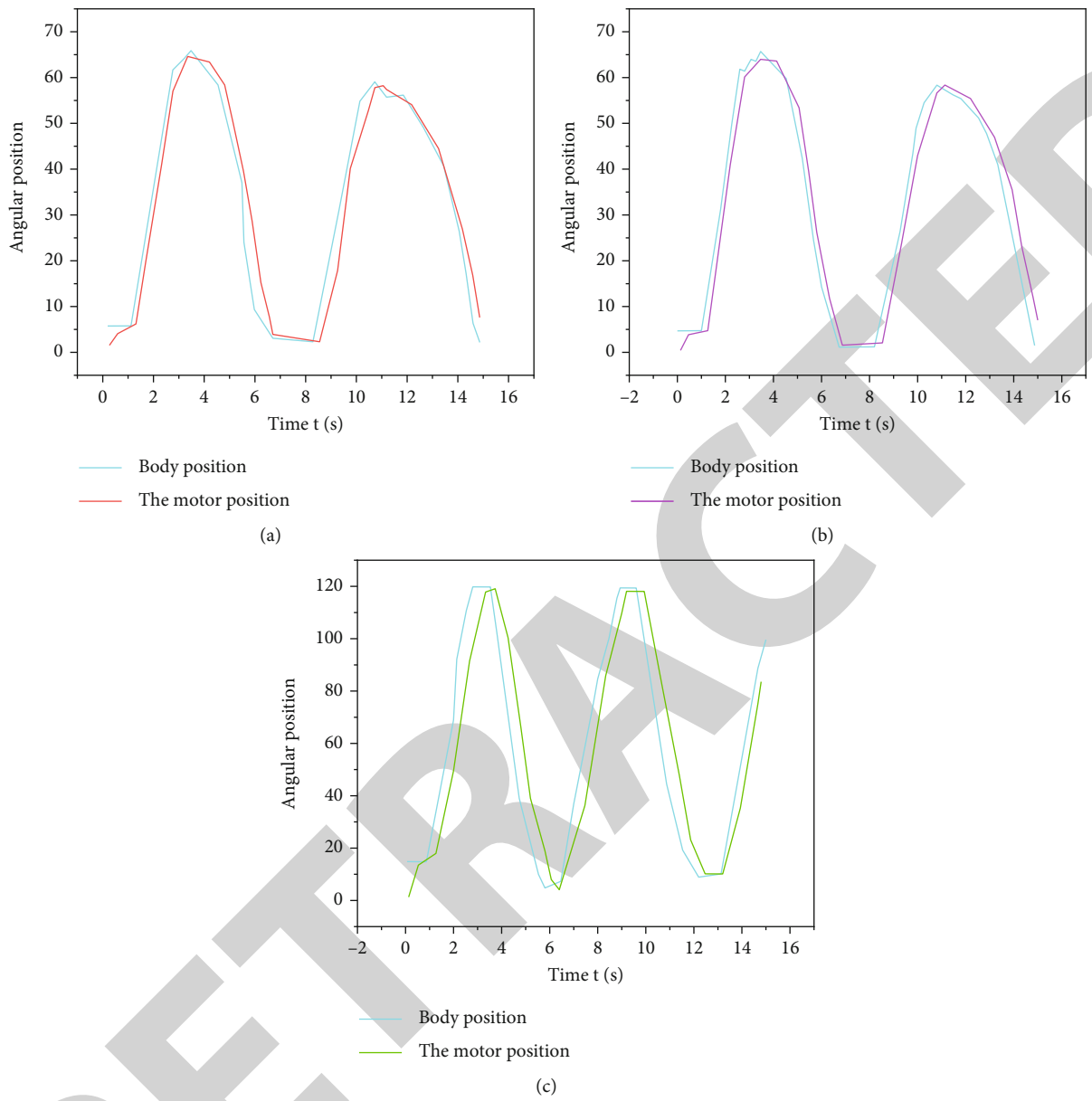

Figure 2: (a) Shoulder abduction/adduction angle curve. (b) Shoulder flexion/extension angle curve. (c) Elbow flexion/extension angle curve.

often not zero, and the drive motors of each axis are at the initial zero position [21]. After a period of exercise, the difference between the two decreased gradually. The horizontal straight line generated by the crest or trough of the curve is due to the limitation of the range of joint movement during data processing, so as to ensure the safe operation of the system. Table 3 shows the average angular velocity of each joint, the average angular error of each joint in a single flexion and extension, and the maximum action delay within a certain period of time.

It can be seen from Table 3 that the greater the angular velocity of the healthy limb joint movement, the greater the error between the angle obtained by the somatosensory and the actual position of the exoskeleton robot arm joint. This is because the refresh rate of the joint angle obtained by Kinect is 30 frames per second, while the position update speed of the motor lags behind under load. With the decrease of joint velocity, the position error and maximum delay decrease, and the follow-up performance is improved. Generally, the joint angular velocity of rehabilitation training is carried out at a low speed below 30°/s. The follow-up performance of each axis of the upper limb exoskeleton rehabilitation robot basically meets the requirements of rehabilitation training.

4. Result Analysis

Considering that the equipment is a kind of monitoring equipment, not a treatment or diagnostic equipment, and the equipment will not exert auxiliary movement effect on

Table 3: Follow-up performance of each joint.

	Average angular velocity (°/s)	Mean value of angle error (°)	Maximum delay (s)
Elbow flexion/extension	34.3	12.3	0.80
Shoulder abduction/adduction	25.6	6.8	0.41
Shoulder flexion/extension	17.3	3.1	0.37

patients, the selection of cases is mainly based on the following two points: ① Patients need to have good movement ability and perform large range of movement in the monitoring process, and ② patients have good compliance and cognitive ability and can wear equipment for a long time to complete monitoring. Disease type, drug treatment, and other factors are not taken as the basis for case selection. Based on the above considerations, three home-based rehabilitation patients with normal cognitive ability were selected for the preliminary experiment. The Brunnstrom stages of upper and lower limbs of the three patients were more than 4 when they left the hospital. They had similar transfer and daily living abilities and were able to wear and use the equipment as required. After the system is deployed in the patient's home, each patient will wear sensors in the morning and afternoon for 2 h of motion capture. During the experiment, the patients received a total of 1H rehabilitation training according to the doctor's requirements, including 20 min treadmill walking training, and could freely move indoors at other times. The experiment lasted for 4 weeks. To ensure the repeatability of the experiment, we selected the walking training with high similarity for the test. When the patient was walking, the speed of the treadmill was set at 3 km/h. In addition to wearing sensors for monitoring, the optical tracking method described in previous studies is also used as a reference, and the walking video is synchronously recorded at a frame rate of 25 Hz. The included angle between the thigh centerline and the vertical direction is measured frame by frame for the obtained video, forming a pitching angle curve as shown by the dotted line in Figure 3 [22]. At the same time, according to the Kalman filter algorithm, the pitch angle curve of the thigh during walking is drawn as a solid line in Figure 3.

The two curves in Figure 3 show the same change trend. The average deviation of the maximum value of the thigh pitch angle monitored by the two methods is 0.063 radians (≈3.6°), the average deviation of the minimum value is 0.067 radians (≈3.8°), and the average difference of the angles of the two curves is 0.072 radians (≈4.1°). In addition to the above clips, after the statistics of the 4-week walking test results of 3 patients, the average difference of thigh pitch angle obtained by the optical and Kalman filtering algorithms is 3.7°, 4.3°, and 4.0°, respectively, with an average of 4.0° [23]. In this study, the maximum delay of the equipment in data transmission is 80 ms, while the TD is 320 ms. The increase of delay is related to the filtering algorithm. The Kalman filter described in this paper adopts the constant angular velocity model. When the angular velocity changes suddenly, the swing velocity of the thigh in this example suddenly increases or decreases, and the angular velocity value and the corresponding covariance matrix need several iterations to match the current motion. The filtering result is expressed as a lag period of time, which also leads to the difference between the measurement and calculation of the angle value at the same time by the above optical and Kalman filtering algorithms [24]. After the statistics of the walking test results of three patients, the maximum delay of the system was 480 ms, with an average of 297 ms.

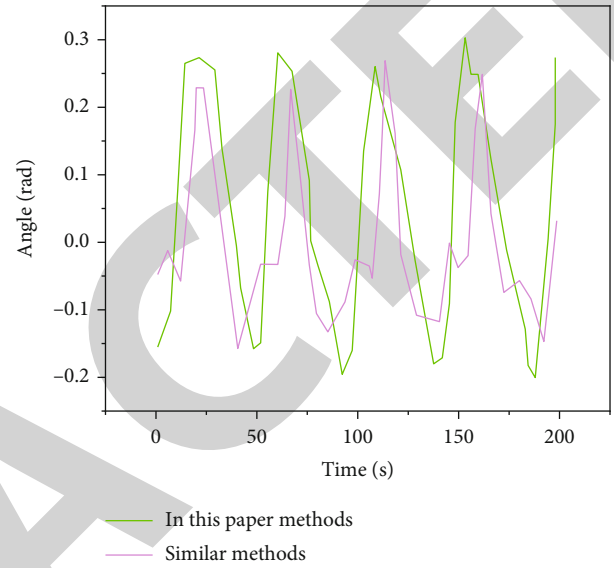

Figure 3: Thigh pitch angle curve during walking.

The rehabilitation doctor's evaluation on the use of the device is also a part of the experiment. The rehabilitation doctor observes the actual action and the model action displayed by the mobile terminal when the patient uses the device. The evaluation conclusions are as follows: ① The model action has a high degree of reduction relative to the actual action of the patient, and the action is accurate and continuous, which can replace manual monitoring, and does not use cameras, and does not infringe on the privacy of the patient; ② the range of motion displayed by the motion reconstruction app is within 5° of the manual measured value, meeting the needs of rehabilitation medicine for motor function evaluation and training guidance; and ③ the system delay is less than 0.5 s, which has good real-time performance and can respond quickly to emergencies, ensuring the safety of patients' out-of-hospital rehabilitation [25].

5. Conclusion

In this research, the customized wearable sensor and universal mobile terminal are used as the hardware. Based on the sensor, the motion capture algorithm and motion reconstruction algorithm are developed. In the initial experimental application, it has been proved that this device can provide stable and accurate real-time motion capture results, provide statistical data that can help rehabilitation doctors conduct functional evaluation, and is of great significance for rehabilitation doctors to formulate training plans and carry out rehabilitation training for patients. It is a crucial attempt in the field of "Internet of things + rehabilitation medicine."

Data Availability

The data used to support the findings of this study are available from the corresponding author upon request.

Conflicts of Interest

The authors declare that they have no conflicts of interest.

Acknowledgments

The study was supported by the Anhui Province Philosophy and Social Science Planning project "Research on the Institutional Guarantee and Policy Support of Mass Sports Development in Anhui Province under the Prethreshold of Comprehensive Well-off society" (AHSKQ2020D108); Key Projects of Humanities and Social Sciences Research in Universities in Anhui Province: Research on high-quality Integrated Development of Sports Industry in the Yangtze River Delta region under the new pattern of "double cycle" (SK2021A0411); Fuyang Normal University 2021 Key Youth Talent Project "Research on the Development Path of Ecological Sports in Anhui Province under the New Normal" (rcxm202115); and Anhui Province Quality Engineering Project: New Liberal Arts, New Medical Research and Reform Practice Project (2020wyxm134).

References

[1] X. Li, Z. Zhu, N. Shen, W. Dai, and Y. Hu, "Deeply feature learning by cmac network for manipulating rehabilitation robots," *Future Generation Computer Systems*, vol. 121, no. 1, pp. 19–24, 2021.

[2] M. Wang, R. Ou, and Y. Wang, "Multiplicatively weighted voronoi-based sensor collaborative redeployment in software-defined wireless sensor networks," *International Journal of Distributed Sensor Networks*, vol. 18, no. 3, article 155014772114057, 2022.

[3] N. D. Silverberg and G. L. Iverson, "Reply to letter to the editor: expert panel survey to update the American congress of rehabilitation medicine definition of mild traumatic brain injury," *Archives of Physical Medicine and Rehabilitation*, vol. 102, no. 6, p. 1239, 2021.

[4] H. Y. Zhao, J. Q. Han, H. T. Liu, Q. Wang, and D. Hu, "Effects of hand continuous passive motion system combined with functional training and pressure gloves in treating early scar contracture after burn on the back of the hand," *Chinese journal of burns*, vol. 37, no. 4, pp. 1–8, 2021.

[5] R. Dionisio, P. Torres, A. Ramalho, and R. Ferreira, "Magnetoresistive sensors and piezoresistive accelerometers for vibration measurements: a comparative study," *Journal of Sensor and Actuator Networks*, vol. 10, no. 1, p. 22, 2021.

[6] D. Chen, Q. Liu, Z. Han et al., "Sensor-actuators: 4D printing strain self-sensing and temperature self-sensing integrated sensor–actuator with bioinspired gradient gaps (Adv. Sci. 13/2020)," *Advanced Science*, vol. 7, no. 13, p. 2070075, 2020.

[7] D. Jang, G. Jung, Y. Jeong, S. Hong, and J. H. Lee, "Barometric pressure sensor with air pocket integrated with mosfets on the same substrate," *Journal of Semiconductor Technology and Science*, vol. 20, no. 3, pp. 305–310, 2020.

[8] Q. Duan, Y. Mao, H. Zhang, and W. Xue, "Add-on integration module-based proportional-integration-derivative control for higher precision electro-optical tracking system," *Transactions of the Institute of Measurement and Control*, vol. 43, no. 6, pp. 1347–1362, 2021.

[9] Y. Yu, R. Chen, L. Chen, W. Li, and H. Zhou, "H-WPS: hybrid wireless positioning system using an enhanced WI-FI FTM/RSSI/MEMS sensors integration approach," *IEEE Internet of Things Journal*, vol. 99, pp. 1–1, 2021.

[10] Y. Bouteraa, I. B. Abdallah, and A. Elmogy, "Design and control of an exoskeleton robot with emg-driven electrical stimulation for upper limb rehabilitation," *Industrial Robot: the international journal of robotics research and application*, vol. 47, no. 4, pp. 489–501, 2020.

[11] X. Chen and Z. Feng, "Order spectrum analysis enhanced by surrogate test and Vold-Kalman filtering for rotating machinery fault diagnosis under time-varying speed conditions," *Mechanical Systems and Signal Processing*, vol. 154, no. 331, p. 107585, 2021.

[12] G. Sonowal and K. S. Kuppusamy, "PhiDMA - a phishing detection model with multi-filter approach," *Journal of King Saud University - Computer and Information Sciences*, vol. 32, no. 1, pp. 99–112, 2020.

[13] G. Kim, S. Y. Lee, J. S. Oh, and S. Lee, "Deep learning-based estimation of the unknown road profile and state variables for the vehicle suspension system," *IEEE Access*, vol. 9, pp. 13878–13890, 2021.

[14] N. Sai, T. Zhang, J. Wu, and W. J. Han, "Noise-induced blood-labyrinth-barrier trauma of guinea pig and the protective effect of matrix metalloproteinase inhibitors," *Chinese journal of otorhinolaryngology head and neck surgery*, vol. 55, no. 4, pp. 363–370, 2020.

[15] S. Elsheikh, A. Fish, and D. Zhou, "Exploiting spatial information to enhance DTI segmentations via spatial fuzzy c-means with covariance matrix data and non-Euclidean metrics," *Applied Sciences*, vol. 11, no. 15, p. 7003, 2021.

[16] G. Gao, S. Gao, G. Hu, and X. Peng, "Spectral redshift observation-based sins/srs/cns integration with an adaptive fault-tolerant cubature Kalman filter," *Measurement Science and Technology*, vol. 32, no. 9, p. 095103, 2021.

[17] E. Angelakis, A. Andreopoulou, and A. Georgaki, "Multisensory biofeedback: promoting the recessive somatosensory control in operatic singing pedagogy," *Biomedical Signal Processing and Control*, vol. 66, no. 3, article 102400, 2021.

[18] G. Dhiman, V. Kumar, A. Kaur, and A. Sharma, "Don: deep learning and optimization-based framework for detection of novel coronavirus disease using x-ray images,"

Interdisciplinary Sciences Computational Life Sciences, vol. 13, no. 2, pp. 260–272, 2021.

[19] P. Ajay, B. Nagaraj, R. A. Kumar, R. Huang, and P. Ananthi, "Unsupervised hyperspectral microscopic image segmentation using deep embedded clustering algorithm," *Scanning*, vol. 2022, Article ID 1200860, 9 pages, 2022.

[20] J. Liu, X. Liu, J. Chen, X. Li, T. Ma, and F. Zhong, "Investigation of ZrMnFe/sepiolite catalysts on toluene degradation in a one-stage plasma-catalysis system," *Catalysts*, vol. 11, no. 7, p. 828, 2021.

[21] G. Veselov, A. Tselykh, A. Sharma, and R. Huang, "Special issue on applications of artificial intelligence in evolution of smart cities and societies," *Informatica (Slovenia)*, vol. 45, no. 5, p. 603, 2021.

[22] H. Xie, Y. Wang, Z. Gao, B. Ganthia, and C. Truong, "Research on frequency parameter detection of frequency shifted track circuit based on nonlinear algorithm," *Nonlinear Engineering*, vol. 10, no. 1, pp. 592–599, 2021.

[23] P. Tucan, C. Vaida, I. Ulinici, A. Banica, and D. Pisla, "Optimization of the aspire spherical parallel rehabilitation robot based on its clinical evaluation," *International Journal of Environmental Research and Public Health*, vol. 18, no. 6, p. 3281, 2021.

[24] V. Bahrami, A. Kalhor, and M. T. Masouleh, "Dynamic modeling and design of controller for the 2-dof serial chain actuated by a cable-driven robot based on feedback linearization," *Proceedings of the Institution of Mechanical Engineers, Part C: Journal of Mechanical Engineering Science*, vol. 236, no. 5, pp. 2546–2558, 2022.

[25] J. Wang, G. Zuo, J. Zhang, C. Shi, and S. Guo, "Research on assist-as-needed control strategy of wrist function-rehabilitation robot," *Journal of biomedical engineering*, vol. 37, no. 1, pp. 129–135, 2020.